

New Spectral State of Supercritical Accretion Flow with Comptonizing Outflow

Tomohisa KAWASHIMA,^{1,2}Ken OHSUGA,^{3,4} Shin MINESHIGE,⁵ Dominikus HEINZELLER,⁵ Hideaki TAKABE,⁶ and Ryoji MATSUMOTO¹

¹*Department of Physics, Graduate School of Science, Chiba University, 1-33 Yayoi-cho, Inage-ku, Chiba 263-8522, Japan*

kawashima-t@astro.s.chiba-u.ac.jp

²*Department of Space and Earth, Graduate School of Osaka University, Toyonaka, Japan*

³*National Astronomical Observatory of Japan, 2-21-1 Osawa, Mitaka-shi, Tokyo 181-8588*

⁴*Institute of Physical and Chemical Research (RIKEN), 2-1 Hirosawa, Wako, Saitama 351-0198, Japan*

⁵*Department of Astronomy, Kyoto University, Kitashirakawa, Sakyo-ku, Kyoto 606-8502, Japan*

⁶*Institute of Laser Engineering, Osaka University, 2-6 Yamada-Oka, Suita, Osaka 565-0871, Japan*

(Received 2000 December 31; accepted 2001 January 1)

Abstract

Supercritical accretion flows inevitably produce radiation-pressure driven outflows, which will Compton up-scatter soft photons from the underlying accretion flow, thereby making hard emission. We perform two dimensional radiation hydrodynamic simulations of supercritical accretion flows and outflows, incorporating such Compton scattering effects, and demonstrate that there appears a new hard spectral state at higher photon luminosities than that of the slim-disk state. In this state, as the photon luminosity increases, the photon index decreases and the fraction of the hard emission increases. The Compton y -parameter is of the order of unity (and thus the photon index will be ~ 2) when the apparent photon luminosity is $\sim 30L_E$ (with L_E being the Eddington luminosity) for nearly face-on sources. This explains the observed spectral hardening of the ULX NGC1313 X-2 in its brightening phase and thus supports the model of supercritical accretion onto stellar mass black holes in this ULX.

Key words: accretion, accretion disks — black hole physics — hydrodynamics — radiative transfer

1. Introduction

It is long known that astrophysical black holes (especially, black hole binaries) exhibit several distinct spectral states. These are, in the order of increasing photon luminosities (see, e.g., Esin et al. 1997): a low/hard state with a hard, power-law-like emission component, a high/soft state with a soft, thermal emission component (e.g., Tananbaum et al. 1972; Dolan et al. 1979), and a very high state showing both spectral components (e.g., Miyamoto et al. 1991; Kubota and Done 2004). In addition, there seems to exist another soft spectral state at even higher photon luminosities, comparable to the Eddington luminosity (L_E), called the slim disk state (Abramowicz et al. 1988; Watarai et al. 2000, see Kato et al. 2008 for a review and references therein). Although recent observations suggest its existence (Vierdayanti et al. 2006; Okajima et al. 2006), a robust observational proof of this state has not yet been obtained.

In this respect it is interesting to note that Ultraluminous X-ray sources (ULXs), which are recently found successively in the off-center region of nearby external galaxies, also show both the soft thermal and the hard power-law spectral states (Makishima et al. 2000; Cropper et al. 2004). Some of them, such as IC342 X-1 and X-2, even show spectral transitions between these two states (Kubota and Makishima 2001). Notably, the typical photon luminosities of ULXs range between $L_{\text{ph}} \simeq 10^{39-41} \text{ erg s}^{-1}$, which exceeds the Eddington luminosity for neutron stars and stellar-mass black holes. There are two possible models considered to account for such large photon luminosities: subcritical accretion (i.e., accretion below the Eddington accretion rate) onto an intermediate-mass black hole (IMBH, Miller et al. 2003; Miller et al. 2004; Cropper et al. 2004; Berghea et al. 2008) and supercritical accretion onto a stellar-mass black hole (King et al. 2001; Ebisawa et al. 2003; Okajima et al. 2006; Tsunoda et al. 2006; Vierdayanti et al. 2006; Poutanen et al. 2007; Vierdayanti et al. 2008). Since the black hole masses of ULXs are poorly known, we cannot discriminate between these two models at present. The study of spectral states and spectral transitions, in analogy to black hole binaries, are one possibility to resolve this issue, but the situation turns out to be very complex. If the two states of ULXs correspond to the low/hard state and the high/soft state, the photon luminosities of ULXs should be sub-Eddington and thus the IMBH hypothesis will be favored. If, on the other hand, the soft state of ULXs corresponds to the slim-disk state, these ULXs should be supercritical sources, which means that the black holes cannot be IMBHs. The proper identification of the spectral states is thus essential for understanding the nature of accretion flows and black holes in ULXs.

Interesting trends have been reported recently. Some ULXs (such as HoIX X-1) show spectral softening when the photon luminosity increases (Kajava & Poutanen. 2008). It is thus natural to conclude that the brighter, soft state corresponds to the slim-disk state. Then, its photon luminosity should be close to the Eddington luminosity, thereby supporting the supercritical hypothesis for ULXs. To our surprise, however, there exists another class of ULXs

(such as NGC1313 X-2) which exhibit the completely opposite behavior; that is, they show spectral hardening as the photon luminosity increase (Roberts et al. 2006; Mizuno et al. 2007). It is then reasonable to conclude that the observed soft-to-hard transitions correspond to the transition from the high/soft state to the very high state in the black hole binaries. In this case, the photon luminosities should be sub-Eddington and, hence, the IMBH model will be favored. However, we can propose another interpretation. If a hard spectral state exists in the supercritical regime and if these sources are in such a very bright phase, the supercritical model will survive. From a theoretical point of view, this seems to be a natural consequence: supercritical accretion flows inevitably produce radiation-pressure driven outflows and such outflows will Compton up-scatter soft photons, thereby making a hard emission component. The higher the photon luminosity is, the harder emission we expect. In this paper we will demonstrate that this is indeed feasible based on new two-dimensional radiation-hydrodynamic (RHD) simulations, which incorporate the Compton scattering effects.

Two-dimensional RHD simulations of supercritical accretion flows around stellar-mass black holes were pioneered by Eggum et al. (1988) and followed by several authors (Okuda 2002; Okuda et al. 2005; Ohsuga 2007a). Supercritical accretion in a quasi-steady state was first calculated by Ohsuga et al. (2005), who found that the total photon luminosities can indeed exceed three times the Eddington luminosity, whereas the apparent photon luminosities become more than ten times larger than the Eddington luminosity for a face-on observer (see also Heinzeller et al. 2006). They have also shown that hot outflows with their gas temperature higher than 10^9 K appear above the disk. This suggests that the inverse Compton scattering of soft disk emission by such high temperature plasmas should be important, though it was not yet studied quantitatively. This motivated us to perform extended simulations that incorporate Compton scattering effects. We find that the higher the mass accretion rate is, more high-temperature gas exists as outflow and, therefore, the larger becomes the Compton y -parameter (see equation (6) in section 3 for the definition of the Compton y -parameter). We thus expect that SED becomes harder when the photon luminosity is higher. This new state will explain the SED variation of some ULXs.

The plan of this paper is as follows: In §2 we present basic equations and numerical methods. In §3 we present the structure of supercritical accretion flows with Comptonizing outflows and compute the Compton y -parameter. Finally, §4 is devoted to discussion of our findings.

2. Methods

Following Ohsuga et al. (2005), but also considering the effects of Compton scattering in the energy exchange between photons and electrons, we solve the RHD equations in spherical coordinates (r, θ, ϕ) . The radiative transfer equation is solved using the flux-limited diffusion approximation (Levermore & Pomraning 1981; Turner & Stone 2001). The general relativistic

effects are incorporated by a pseudo-Newtonian potential, $\Psi = -GM/(r - r_s)$ (Paczynsky & Wiita 1980), where $r_s (= 2GM/c^2)$ is the Schwarzschild radius, G is the gravitational constant, M is the mass of the black hole ($M = 10M_\odot$ is employed), and c is the speed of light. We assume that the flow is non-self gravitating, axisymmetric with respect to the rotation axis (i.e., $\partial/\partial\phi = 0$), and symmetric relative to the equatorial plane (where $\theta = \pi/2$). We also adopt the α viscosity prescription (Shakura & Sunyaev 1973) and set $\alpha = 0.1$.

The basic equations are the same as those in Ohsuga et al. (2005) except that we add Compton heating/cooling terms in the energy equations of gas and radiation;

$$\frac{\partial e}{\partial t} + \nabla \cdot (e\mathbf{v}) = -p\nabla \cdot \mathbf{v} - 4\pi\kappa B + c\kappa E_0 + \Phi_{\text{vis}} - \Gamma_{\text{Comp}}, \quad (1)$$

$$\frac{\partial E_0}{\partial t} + \nabla \cdot (E_0\mathbf{v}) = -\nabla \cdot \mathbf{F}_0 - \nabla \mathbf{v} \cdot \mathbf{P}_0 + 4\pi\kappa B - c\kappa E_0 + \Gamma_{\text{Comp}}. \quad (2)$$

Here $\mathbf{v} = (v_r, v_\theta, v_\phi)$ is the velocity, p is the gas pressure, e is the internal energy density of the gas, B is the blackbody intensity, E_0 is the radiation energy density, where the suffix 0 represents quantities in the comoving frame. $\mathbf{F}_0 = (F_0^r, F_0^\theta)$ is the radiative flux, \mathbf{P}_0 is the radiation pressure tensor, Γ_{Comp} is the energy transport rate from the gas to the radiation field via the Comptonization, κ is the absorption opacity, and Φ_{vis} is the viscous dissipation function. We write Γ_{Comp} as

$$\Gamma_{\text{Comp}} = 4\sigma_T c \frac{k_B(T_{\text{gas}} - T_{\text{rad}})}{m_e c^2} \left(\frac{\rho}{m_p} \right) E_0, \quad (3)$$

where T_{gas} is the gas temperature, $T_{\text{rad}} [= (E_0/a)^{1/4}]$ is the radiation temperature, a is the radiation constant, ρ is the mass density of the gas, σ_T is the cross section for electron scattering, m_e is the electron mass, and m_p is the proton mass. We assume a one-temperature plasma in which the electron temperature equals the ion temperature. This equation is obtained by integrating the Kompaneets equation over the frequency (see e.g., Padmanabhan 2000 for detail).

Our methods are the same as Ohsuga (2006) except that we solve the energy equations including the Compton heating/cooling terms. We employ the operator-splitting method in the energy equations and additionally solve the following equations;

$$\frac{\partial e}{\partial t} = -\Gamma_{\text{Comp}}, \quad (4)$$

$$\frac{\partial E_0}{\partial t} = \Gamma_{\text{Comp}}, \quad (5)$$

using Newton-Raphson iteration, with bisection when Newton-Raphson method fails.

We start the calculations with a hot, rarefied, optically thin atmosphere (i.e., without an initial optically thick disk). We solve the RHD equations numerically by an explicit-implicit finite-difference scheme on an Eulerian grid. The computational domain size is $3r_s \leq r \leq 500r_s$ and $0 \leq \theta \leq \pi/2$. We imposed an absorbing boundary condition at $r = r_{\text{in}} = 3r_s$ by attaching a damping layer, in which the physical quantities q gradually approach the initial values q_0 as

$q_{\text{new}}(i - n) = q(i) - (q(i) - q_0)f(n)$, where $r(i) = r_{\text{in}}$. The function $f(n)$ is a smooth function which monotonically increases from 0 to 1 as n increases. We continuously add mass through the outer boundary ($r = r_{\text{out}} = 500r_s$) near the equatorial plane ($0.45\pi \leq \theta \leq 0.5\pi$) at a constant rate \dot{m}_{input} . Here, \dot{m}_{input} is the mass input rate normalized by the critical accretion rate, $\dot{M}_{\text{crit}} \equiv L_E/c^2$. The injected matter is assumed to have a specific angular momentum corresponding to the Keplerian angular momentum at $r = 100r_s$. On the other hand, we allow matter to escape freely but not to enter the computational domain at $r = r_{\text{out}}$ and $0 \leq \theta < 0.45\pi$. The number of grid points is $(N_r, N_\theta) = (96, 96)$. The grid points in the radial direction are distributed such that $\Delta \ln r = \text{constant}$, while the grids in θ direction are distributed in such a way that $\Delta \cos \theta = 1/N_\theta$.

3. Numerical Results

3.1. Quasi-Steady Structure

We first overview the accretion flow and outflow properties. The overall evolution can be classified into two phases: a transient accumulation phase and a subsequent quasi-steady phase. In the former one, matter injected through the outer disk boundary creates continuous gas inflow and accumulates around $r = 100r_s$, where the angular momentum of the injected gas equals that of the Keplerian rotation. Viscous processes allow the angular momentum of the gas to be transported outward, which drives the gas inflow. Eventually, the gas falls onto the black hole in a quasi-steady fashion. In this subsection, we fix the mass input rate at the outer boundary to a value $\dot{m}_{\text{input}} = 10^3$.

Figure 1 shows the color contours of the gas temperature (top panels) and of the mass density overlaid with the fluid velocity vectors (bottom panels) in the quasi-steady state for models with and without Comptonization in the left and right panels, respectively. We easily notice that the gas temperature of the outflow, which was originally 10^9 – 10^{11} K (Fig. 1b), is now reduced considerably to $\sim 10^{7.5}$ – 10^8 K, when we take into account the Comptonization effects (Fig. 1a). The gas temperature in the disk region, on the other hand, does not change appreciably. This is because the radiation temperature and the gas temperature are nearly equal due to frequent absorption and emission of photons in the disk. The ratio of the Compton cooling timescale ($t_{\text{Comp}} \sim e/|\Gamma_{\text{Comp}}|$) to the cooling timescale by the free-free and bound-free emission ($t_{\text{ff,bf}} \sim e/|4\pi\kappa B - c\kappa E_0|$) is $t_{\text{Comp}}/t_{\text{ff,bf}} \sim 10^{-5}$ in the outflow region and ~ 1 in the disk region. We also note that in the outflow region the ratio of the Compton cooling timescale to the escaping timescale of the outflow ($t_{\text{esc}} \sim r_{\text{out}}/0.1c$) is $t_{\text{Comp}}/t_{\text{esc}} \sim 10^{-4}$ although that of the cooling timescale by free-free and bound-free emission to the escaping timescale is $t_{\text{ff,bf}}/t_{\text{esc}} \sim 10^1$. Therefore the outflowing gas is efficiently cooled by the Comptonization before the gas escape from computational domain (by contraries, the cooling by free-free and bound-free emission is not effective in the outflow region).

The outflowing gas is less dense in models including the Comptonization. A reduction in the outflow rate leads to an increase of the mass accretion rate onto the black hole and leads to a geometrically thicker accretion flow.

We find that the accretion rate onto the black hole and the total viscous heating rate in the model with Compton cooling are larger than those in the model without Compton cooling by about 70% and 20%, respectively. The disk scale height is decreased by the Compton cooling in the outflow region. Therefore, the gas above the disk accumulates towards the disk plane (The radiative force in the disk region is reduced due to photon diffusion processes). Compared with the case without Comptonization, the amount of the radiation-pressure driven outflow is smaller, the mass accretion rate is larger, and the viscous heating rate is also larger in the case with Comptonization. The photon luminosity remains about the same, however. The energy of the photons which are swallowed by the black hole per unit time in the model with Comptonization is three times as large as that without Comptonization. The increase in the mass accretion rate makes photon-trapping effects more significant (Ohsuga et al. 2002). Most of the photons which are produced additionally by the inclusion of the Compton effects are generated around the innermost region of the accretion disk (i.e., in the photon-trapping region). Thus, they are swallowed by the black hole without escaping to the outflow region (Ohsuga and Mineshige 2007). This is the reason why the observed photon luminosity does not change appreciably by the inclusion of the Compton effects.

3.2. Hardness of the Photon Spectrum

The Compton cooling of the outflow region affects the radiation spectra. In this subsection, we use time-averaged simulation results to discuss the spectral properties in terms of the Compton y -parameter, which indicates how much seed soft photons are up-scattered by the hot electrons in the outflow. The y -parameter is given by

$$y = \frac{4k_B T_e}{m_e c^2} \max(\tau_{\text{es}}, \tau_{\text{es}}^2), \quad (6)$$

where τ_{es} is the Thomson optical depth of the outflow. Note that we assume a one-temperature plasma and, hence, electron and proton temperatures are the same in this paper.

We calculate the Compton y -parameter in the following way. First, we specify a ray, a straight line that connects a point at the outer boundary (r_{out}, θ) and the origin $(r=0)$ with an inclination angle of θ (measured with respect to the z -axis). Second, we define a photosphere for that ray by the position where $\tau_{\text{eff}}(\theta) = \sqrt{\tau_a(\theta)(\tau_a(\theta) + \tau_{\text{es}}(\theta))} = 1$. Here the optical depth for absorption $\tau_a(\theta)$ and for electron scattering $\tau_{\text{es}}(\theta)$ are integrated from the outer boundary of the computational domain. This segment between the photosphere and the outer boundary is used to compute the y -parameter. If the medium along the ray is optically thin, we integrate the opacity inwards to the inner boundary. Third, we obtain the opacity-weighted mean plasma temperature along the ray outside the photosphere by

$$T_e = \frac{\sum T_{\text{gas}}(r_i, \theta) \Delta \tau_{\text{es}}(r_i, \theta)}{\tau_{\text{es}}}, \quad (7)$$

where $\Delta \tau_{\text{es}}(r_i, \theta)$ is the electron scattering opacity in the i -th grid point along the ray, and $\tau_{\text{es}} = \sum \Delta \tau_{\text{es}}(r_i, \theta)$. By separating the summation along the ray to the high temperature region up-scattering photons ($T_e > 10^7$ K) and the low temperature region down-scattering photons ($T_e < 10^7$ K), we confirm that the contribution to the y -parameter from the low temperature region is less than 1. Thus we include only the grid points where $T_{\text{gas}}(r_i, \theta) > 10^7$ K to compute T_e , τ_{es} , and y in equation 6. Otherwise, y will be overestimated. Figure 2 shows the y -parameters in the outflow region. The solid curves show the results for models with Comptonization for various mass input rates, whereas the dashed curve shows the y -parameter for a model without Comptonization. When we include Comptonization effects in the RHD simulation, the y -parameter decreases from $\gtrsim 10^3$ to 10^{-2} – 10^0 because the gas temperature and the gas density in the outflow region decrease (see Fig. 1). Importantly, we confirm that the Compton y -parameter in models with Comptonization is consistent with the observations of ULXs, while that in models without Comptonization is too large to explain them. We also find that the y -parameter increases with an increase of \dot{m}_{input} (and, hence, an increase of the photon luminosity). This is because the larger \dot{m}_{input} is, the larger becomes the electron number density, and, hence, the larger becomes the Thomson optical depth. The SED becomes harder as the photon luminosity increases.

Table 1 summarizes the photon index Γ , the y -parameter, the Thomson optical depth τ_{es} , the averaged gas temperature T_e , and the normalized isotropic (apparent) photon luminosity $L_{\text{ph(iso)}}/L_E$, for a single ray with an angle of $\theta/(\pi/2) \sim 0.05$ (i.e., nearly face-on view). Here we calculate the isotropic photon luminosity by $L_{\text{ph(iso)}} \equiv 4\pi(r_{\text{out}})^2 F_0^r(r_{\text{out}}, \theta)$. The photon index $\Gamma (= -1/2 + \sqrt{9/4 + 4/y})$ resulting from the unsaturated Comptonization (Rybicki & Lightman 1979) is computed using the y -parameter at $\theta/(\pi/2) \sim 0.05$. In Table 1, we also present the normalized kinetic luminosity L_{kin}/L_E , the normalized photon luminosity L_{ph}/L_E , the mass accretion rate onto the black hole $\dot{m} (\equiv \dot{M}/\dot{M}_{\text{crit}})$, the mass outflow rate $\dot{m}_{\text{outflow}} (\equiv \dot{M}_{\text{outflow}}/\dot{M}_{\text{crit}})$, which are integrated over the all angle. The kinetic luminosity is defined as the mechanical energy of outflow which exceed the escape velocity v_{esc} at the outer boundary ($r = r_{\text{out}}$):

$$L_{\text{kin}} \equiv (r_{\text{out}})^2 \int \frac{1}{2} \rho(r_{\text{out}}, \theta) v_r(r_{\text{out}}, \theta)^3 d\Omega. \quad (8)$$

The mass accretion rate is defined at the inner boundary as

$$\dot{M} \equiv (r_{\text{in}})^2 \int \rho(r_{\text{in}}, \theta) \max[-v_r(r_{\text{in}}, \theta), 0] d\Omega. \quad (9)$$

The mass outflow rate is evaluated at the outer boundary:

$$\dot{M}_{\text{outflow}} \equiv (r_{\text{out}})^2 \int \rho(r_{\text{out}}, \theta) \max[v_r(r_{\text{out}}, \theta), 0] d\Omega. \quad (10)$$

Figure 3 shows the dependence of the space-averaged gas temperature of the outflow, the Thomson optical depth, the y -parameter, and the photon index for an observer located in the

direction of $\theta/(\pi/2) \sim 0.05$ on the isotropic photon luminosity. We find a negative correlation between Γ and $L_{\text{ph(iso)}}$. This is because $\max(\tau_{\text{es}}, \tau_{\text{es}}^2)$ increases with an increase of \dot{m} .

4. Discussion

As mentioned in § 1, we expect a hard spectral state exists in the supercritical regimes for the supercritical accretion model for ULXs (i.e., central black holes are stellar-mass black holes) to be viable. In this paper, we demonstrated that such a hard state can really appear in the case of the supercritical accretion onto black holes as a result of the combination of an optically thick, slim-disk type inflow and a Comptonizing outflow. In this new supercritical state, higher photon luminosities correspond to harder SEDs, in analogy to black hole binaries in the very high state, but at even higher photon luminosities.

Figure 4 illustrates schematically our proposed scenario for the variations in the disk geometry and the spectral properties according to the changes in the mass input rate. From top to bottom: (a) Comptonizing outflow state, (b) slim disk state, (c) very high state, and (d) high/soft state. In the slim disk state, in which the photon luminosity barely exceeds L_E , the amount of gas outflow is negligible. Hence, a pure thermal emission component is detectable. However, as the mass input rate increases, the amount of radiation-pressure driven, mildly hot ($\sim 10^{7.5-8}$ K) outflow increases, thereby more soft photons from the accretion flow being Compton up-scattered. The higher the accretion rate is, the harder becomes the SED. This transition can account for the spectral transition reported for some ULXs (e.g., NGC1313 X-2), which show a positive correlation between the SED hardness and the photon luminosity.

What will be an observational test of our proposed spectral state? Unfortunately, line absorption by the outflow material is not expected, since the temperature of the Comptonizing outflow is so high that all the metals in the Comptonizing outflow are completely ionized. Instead, we might search for sources which show both slim-disk features and a Comptonized blackbody component. The slim-disk features can be evaluated through the spectral fitting by using the extended disk-blackbody (DBB) model (Mineshige et al. 1994), in which the temperature profile is assumed to be proportional to r^{-p} , with r being the distance to the central black hole and p being a fitting parameter. The p -value depends on the disk model: $p=0.75$ in the standard-type disk and $p=0.5$ in the slim disk (see Chap. 10 of Kato et al. 2008). Using this technique, Vierdayanti et al. (2006) found that at least some ULXs are powered by supercritical accretion onto stellar-mass black holes. If there are ULXs which show both a soft component with $p=0.5$ and a Comptonized hard component, they will provide strong support for our model.

Next, let us discuss the effect of the bulk (motion) Comptonization. The bulk Comptonization becomes significant when the speed of the bulk motion becomes relativistic. The bulk Comptonization dominates the thermal Comptonization when $\xi \equiv v/(12k_B T_{\text{gas}}/m_e)^{1/2} > 1$ (Blandford and Payne 1981). In our simulation results, the outflow

velocity is $\sim 0.5 c$, while the gas temperature is $\sim 10^{7.5-8}$ K, giving rise to $\xi \sim 1$ in the region near the polar axis. This means that the bulk motion Comptonization is not negligible, compared with the thermal Comptonization. We calculate the y -parameter of bulk Comptonization by $y_{\text{bulk}} = (m_e v^2 / 3m_e c^2) \max(\tau_{\text{es}}, \tau_{\text{es}}^2)$, finding that bulk Comptonization becomes comparable to thermal Comptonization in the region around the polar axis. Hence, we expect substantial bulk Comptonization effects in the spectra of nearly face-on sources. Caution should be taken here, however. Our simulations are likely to overestimate the bulk velocity of the outflow, since the effect of the radiation drag, which decelerates the hydrodynamic motion, is not considered in our code. On the other hand, we evaluate the radiation temperature as $T_{\text{rad}} = (E_0/a)^{1/4}$, which results in underestimation of the radiation temperature, when the radiation spectra become harder than a Planck distribution. Therefore, we may overestimate the cooling rate of the gas via Comptonization, and, hence, underestimate the gas temperature. To evaluate the effects of bulk Comptonization more accurately, full non-gray RHD simulations are required. Future advances in computer technology will enable the study of full non-gray RHD simulations of supercritical accretion flows. We should also note that exponential 'photon breeding' mechanism, which converts a kinetic energy of a relativistic jet into a radiation energy via the bulk Comptonization by electron-positron pair plasmas in a jet (this is a positive feedback mechanism because pair plasma is created by high energy photons), is not efficient. This is because the outflow speed obtained in this study is about $0.5c$ although exponential photon breeding requires highly relativistic motion whose Lorentz factor Γ exceeds 3-4 (Stern & Poutanen 2006).

We showed that in supercritical accretion flows, the kinetic luminosity of the outflow L_{kin} is 0.075, 0.30, 0.55, 1.1 L_E for $\dot{m}_{\text{input}} = 3 \times 10^2, 10^3, 3 \times 10^3, 10^4$ respectively (see Table 1) and that the momentum flux of the outflow is $\sim 2L_{\text{kin}}/v \sim 0.2 - 2 L_E/v \sim L_E/c$, where v ($\sim 0.5c$) is the outflow velocity. The mass, momentum, and energy outflow from the accreting black holes can affect the surrounding interstellar gas. This feedback has been discussed in supermassive black holes (AGN feedback) and should also be relevant in Galactic microquasars. By assuming that the momentum flux of the outflow is $\sim L_E/c$ as suggested by King and Pounds (2003), King (2003, 2005) showed that outflows from a supercritically accreting black hole at the center of the galaxy create a bubble, inside which stars are formed. This mechanism can explain the relation between the black hole mass and the velocity dispersion of the bulge ($M - \sigma$ relation). The results of our simulations for $\dot{m}_{\text{input}} = 10^3$ and 3×10^3 are consistent with the assumptions of King (2003, 2005), if the black hole at the galactic center is accreting the gas supercritically. We note that compared to Ohsuga (2007b), which performed two-dimensional RHD simulations without Comptonization, higher mass input rate is required in our simulations to launch the outflow with the momentum flux $\sim L_E/c$. This is because the mass outflow rate decreases when Comptonization is included, as we mentioned in §3.1.

In this paper we simply assumed the α -prescription of the viscosity. However, it is now widely accepted that the MHD turbulence driven by the magneto-rotational instability (MRI)

provides a promising mechanism for the angular momentum transport in high-temperature flows (Balbus and Hawley 1991; Hawley et al. 1995; Balbus and Hawley 1998). In addition, the Parker instability, driven by the magnetic buoyancy (Parker 1966), creates magnetic loops in the disk corona (Machida et al. 2000). In order to investigate supercritical accretion phenomena without introducing the α -viscosity, we need to perform global radiation magnetohydrodynamic (RMHD) simulations (such simulations are pioneered by Ohsuga et al. (2009), but Compton effects are not included). To treat the relativistic effects of RHD such as radiation drag, it is also necessary to extend our numerical model of the radiative transfer to be valid up to $v/c \sim 1$. This remains as future work.

We would like to thank T. Hanawa, S. Hirose, T. N. Kato, H. Oda, T. Sano, H. Takahashi, and S. Takeuchi for helpful conversations. Numerical simulations were carried out on Cray XT4 at Center for Computational Astrophysics of National Astronomical Observatory of Japan and on Express5800/120Rg-1 at Cybermedia Center Osaka University. This work is supported in part by Ministry of Education, Culture, Sports, Science, and Technology (MEXT) Young Scientist (B) 20740115 (KO), by the Grant-in-Aid of MEXT (19340044, SM, 20340040, RM), and by the Grant-in-Aid for the global COE programs on "The Next Generation of Physics, Spun from Diversity and Emergence" from MEXT (SM, DH).

References

Abramowicz, M. A., Czerny, B., Lasota, J. P., & Szuszkiewicz 1988, *ApJ*, 332, 646
 Balbus, S. A., & Hawley, J. F. 1991, *ApJ*, 376, 214
 Balbus, S. A., & Hawley, J. F. 1998, *Reviews of Modern Physics*, 70, 1
 Berghea, C. T., Wearer, K. A., Colbert, E. J. M., & Roberts, T. P. 2008, *ApJ*, 687, 471
 Blandford, R. D., & Payne, D. G. 1981, *MNRAS*, 194, 1033
 Cropper, M., Soria, R., Mushotzky, R. F., Wu, K., Markwardt, C. B., & Pakull, M. 2004, *MNRAS*, 349, 39
 Dolan, J. F., Grannell, C. J., Dennis, B. R., Frost, K. J., & Orwig, L. E. 1979, *ApJ*, 230, 551
 Ebisawa, K., Źycki, P., Kubota, A., Mizuno, T., & Watarai, K. 2003, *ApJ*, 597, 780
 Eggum, G. E., Coroniti, F. V., & Katz, J. I. 1988, *ApJ*, 330, 142
 Esin, A. A., McClintock, J. E., & Narayan, R. 1997, *ApJ*, 489, 865
 Hawley, J. F., Gammie, C. F., & Balbus, S. A. 1995, *ApJ*, 440, 742
 Heinzeller, D., Mineshige, S., & Ohsuga, K. 2006, *MNRAS*, 372, 1208
 Kato, S., Fukue, J., & Mineshige, S. 2008, *Black-Hole Accretion Disks Towards a New Paradigm* (Kyoto: Kyoto University Press)
 Kajava, J. J. E., & Poutanen, J.:astro-ph/0809.4634(2008)
 Kubota, A., & Makishima, K. 2001, *ApJ*, 547, 119
 King, A. R., Davies, M. B., Ward, M. J., Fabbiano, G., & Elvis, M. 2001, *ApJ*, 552, 109
 King, A. R. 2003, *ApJ*, 596, 27

King, A. R., & Pounds, K.A. 2003, MNRAS, 345, 657

King, A. R. 2005, ApJ, 635, 121

Kubota, A., & Done, C. 2004, MNRAS, 353, 980

Levermore, C. D., & Pomraning, G. C. 1981, ApJ, 248, 321

Makishima, K. et al. 2000, ApJ, 535, 632

Machida, M., Hayashi, M., & Matsumoto, R. 2000, ApJ, 532, 67

Miller, J. M., Fabbiano, G., Miller, M. C. & Fabian, A. C. 2003, ApJ, 585, 37

Miller, J. M., Fabian, A. C., & Miller, M. C. 2004, ApJ, 614, 117

Mineshige, S., Hirano, A., Kitamoto, S., Yamada, T., & Fukue, J. 1994, ApJ, 426, 308

Miyamoto, S., Kimura, K., Kitamoto, S., Dotani, T., & Ebisawa, K. 1991, ApJ, 383, 784

Mizuno, T. et al. 2007, PASJ, 59, 257

Ohnuga, K., Mineshige, S., Mori, M., & Umemura, M. 2002, ApJ, 574, 315

Ohnuga, K., Mori, M., Nakamoto, T., & Mineshige, S. 2005, ApJ, 628, 368

Ohnuga, K. 2006, ApJ, 640, 923

Ohnuga, K. 2007a, PASJ, 59, 1033

Ohnuga, K. 2007b, ApJ, 659, 205

Ohnuga, K., & Mineshige, S. 2007, ApJ, 670, 1283

Ohnuga, K., Mineshige, S., Mori, M., & Kato, Y. 2009, PASJ, in press

Okajima, T., Ebisawa, K., & Kawaguchi, T. 2006, ApJ, 652, 1050

Okuda, T. 2002, PASJ, 54, 253

Okuda, T., Teresi, V., Toscano, E., & Molteni, D. 2005, MNRAS, 357, 295

Paczynsky, B., & Wiita, P. J. 1980, A&A, 88, 23

Padmanabhan, T. 2000, *Theoretical Astrophysics Vol 1: Astrophysical processes* (Cambridge: Cambridge Univ. Press)

Parker, E. N. 1966, ApJ, 145, 811

Poutanen, J., Lipunova, G., Fabrika, S., Butkevich, A. G., & Abolmasov, P. 2007, MNRAS, 377, 1187

Roberts, T. P., Kilgard, R. E., Warwick, R. S., Goad, M. R., & Ward, M. J. 2006, MNRAS, 371, 1877

Rybicki, G. B., & Lightman, A. P. 1979, *Radiative Processes in Astrophysics* (New York: Wiley)

Shakura, N. I., & Sunyaev, R. A. 1973, A&A, 24, 337

Stern, B. E., & Poutanen, J. 2006, MNRAS, 372, 1217

Tananbaum, H., Gursky, H., Kellogg, E., Giacconi, R., & Jones, C. 1972, ApJ, 177, 5

Tsunoda, N., Kubota, A., Namiki, M., Sugiho, M., Kawabata, K., & Makishima, K. 2006, PASJ, 58, 1081

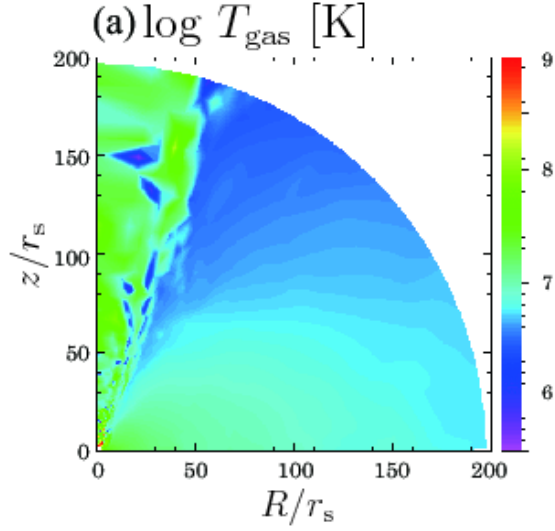
Turner, N. J., & Stone, J. M. 2001, ApJS, 135, 95

Vierdayanti, K., Mineshige, S., Ebisawa, K., & Kawaguchi, T. 2006, PASJ, 58, 915

Vierdayanti, K., Watarai, K., & Mineshige, S. 2008, PASJ, 60, 653

Watarai, K., Fukue, J., Takeuchi, M., & Mineshige, S. 2000, PASJ, 52, 133

with Comptonization



without Comptonization

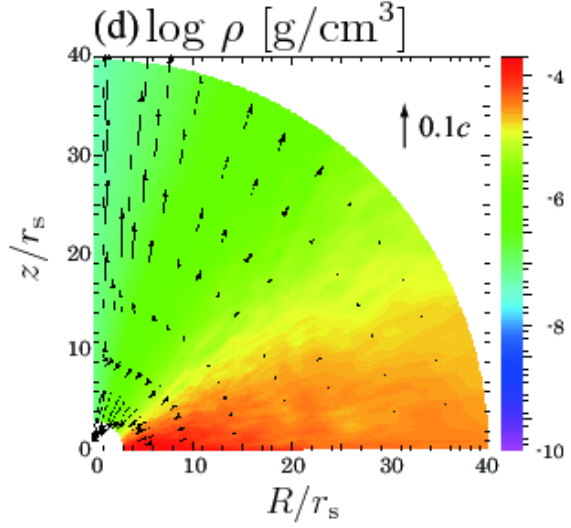
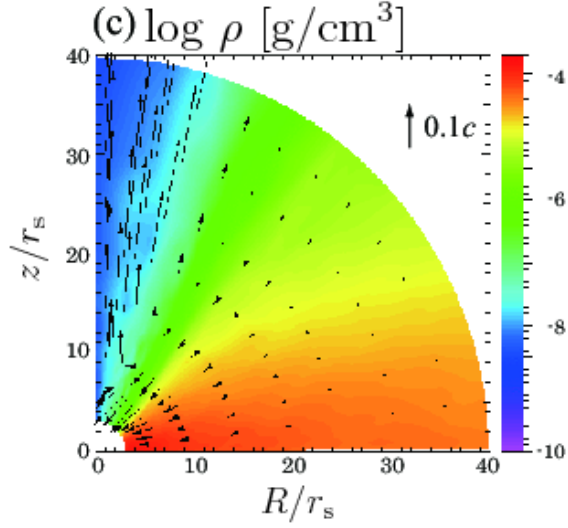
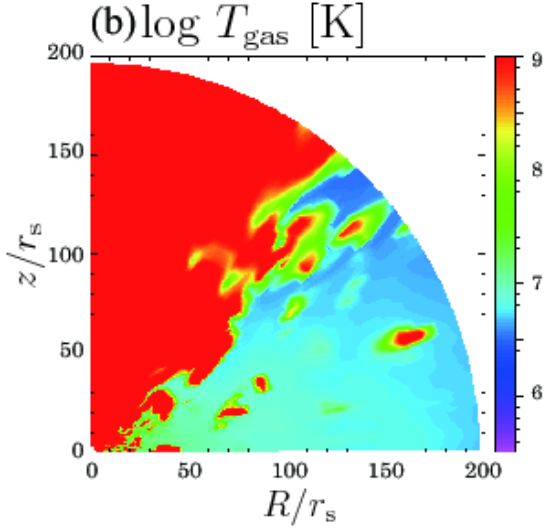


Fig. 1. Distribution of temperature at $t = 40$ s (top) and mass density averaged during $t = 30\text{--}50$ s (bottom). (Left) The model including Comptonization. (Right) The model without Comptonization. Arrows represent velocities of fluid motions.

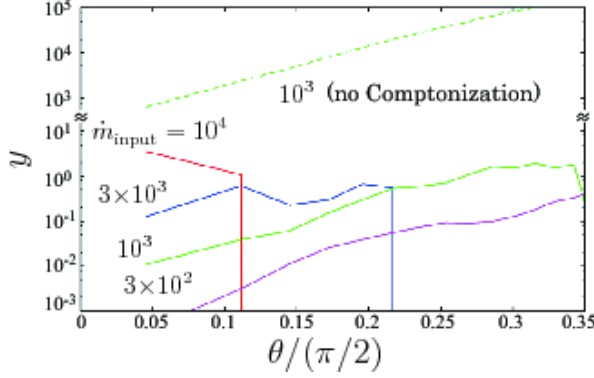


Fig. 2. Compton y -parameter in the outflow region with respect to the polar angle $\theta/(\pi/2)$ for $\dot{m}_{\text{input}} = 3 \times 10^2$ (red), 10^3 (green), 3×10^3 (blue), and 10^4 (magenta). Solid curves represent results for models with Comptonization, the dashed curve shows the results for the model without Comptonization. The y -parameters become zero when $\theta/(\pi/2) \gtrsim 0.12$ and $\gtrsim 0.22$ for $\dot{m}_{\text{input}} = 3 \times 10^3$ and 10^4 , respectively. This is because the gas temperature of the outflow is below 10^7 K.

Table 1. Mass accretion rate, mass outflow rate, luminosities and properties of Comptonizing outflows.*

\dot{m}_{input}	\dot{m}	\dot{m}_{outflow}	L_{kin}/L_E	L_{ph}/L_E	$L_{\text{ph(iso)}}/L_E$	$\max(\tau_{\text{es}}, \tau_{\text{es}}^2)$	T_e	y	Γ
3×10^2	1.3×10^2	3.7×10^1	0.075	2.4	3.6	1.5×10^{-2}	3.7×10^7	3.8×10^{-4}	100
10^3	2.4×10^2	7.5×10^2	0.30	3.2	11	3.9×10^{-1}	4.2×10^7	1.1×10^{-2}	19
3×10^3	4.9×10^2	2.5×10^3	0.55	4.5	21	4.4×10^0	8.3×10^7	2.5×10^{-1}	3.8
10^4	1.3×10^3	8.6×10^3	1.1	8.8	39	1.1×10^2	6.0×10^7	4.4×10^0	1.3

* \dot{m}_{input} is mass input rate, \dot{m} is mass accretion rate, \dot{m}_{outflow} is mass outflow rate, L_{kin} is kinetic luminosity, L_{ph} is photon luminosity, $L_{\text{ph(iso)}}$ is isotropic photon luminosity, L_E is Eddington luminosity, τ_{es} is Thomson optical depth, T_e is electron temperature, y is Compton y -parameter, and Γ is photon index, respectively. We note that \dot{m} , \dot{m}_{outflow} , L_{kin} , and L_{ph} are integrated over the all angle. By contrast, $L_{\text{ph(iso)}}$ is evaluated by $L_{\text{ph(iso)}} = 4\pi(r_{\text{out}})^2 \cdot F_0^r(r_{\text{out}}, \theta)$, where $\theta/(\pi/2) \sim 0.05$. The quantities $\max(\tau_{\text{es}}, \tau_{\text{es}}^2)$, T_e , y and Γ are also evaluated at $\theta/(\pi/2) \sim 0.05$.

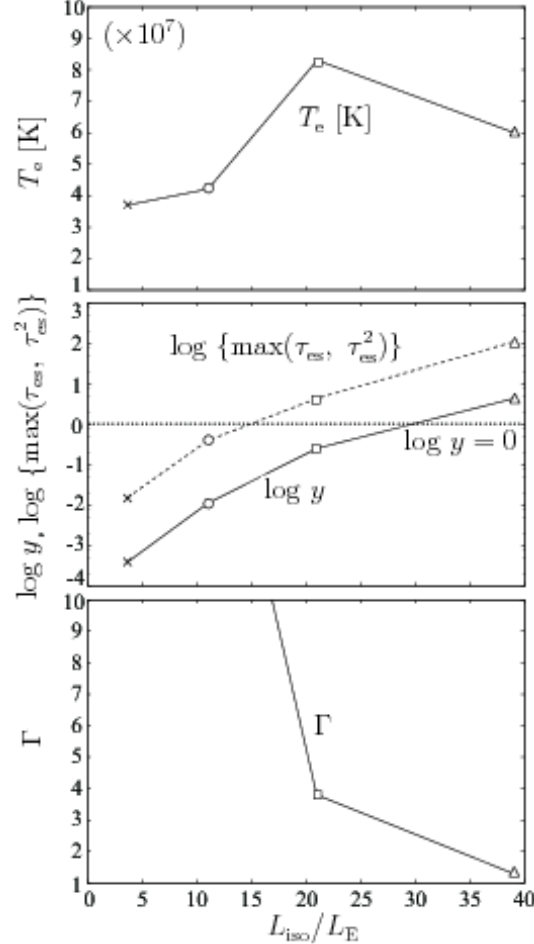


Fig. 3. The gas temperature of outflow averaged along the ray outside the photosphere T_e (top panel), y-parameter, Thomson optical depth $\max(\tau_{\text{es}}, \tau_{\text{es}}^2)$ (middle panel), and the photon index Γ (bottom panel) as functions of photon luminosity L_{ph}/L_E at $\theta/(\pi/2) \sim 0.05$. (Cross: $\dot{m}_{\text{input}} = 3 \times 10^2$, Circle: $\dot{m}_{\text{input}} = 10^3$, Square: $\dot{m}_{\text{input}} = 3 \times 10^3$, Triangle: $\dot{m}_{\text{input}} = 10^4$). The dotted line in the middle panel represents $y = 1$.

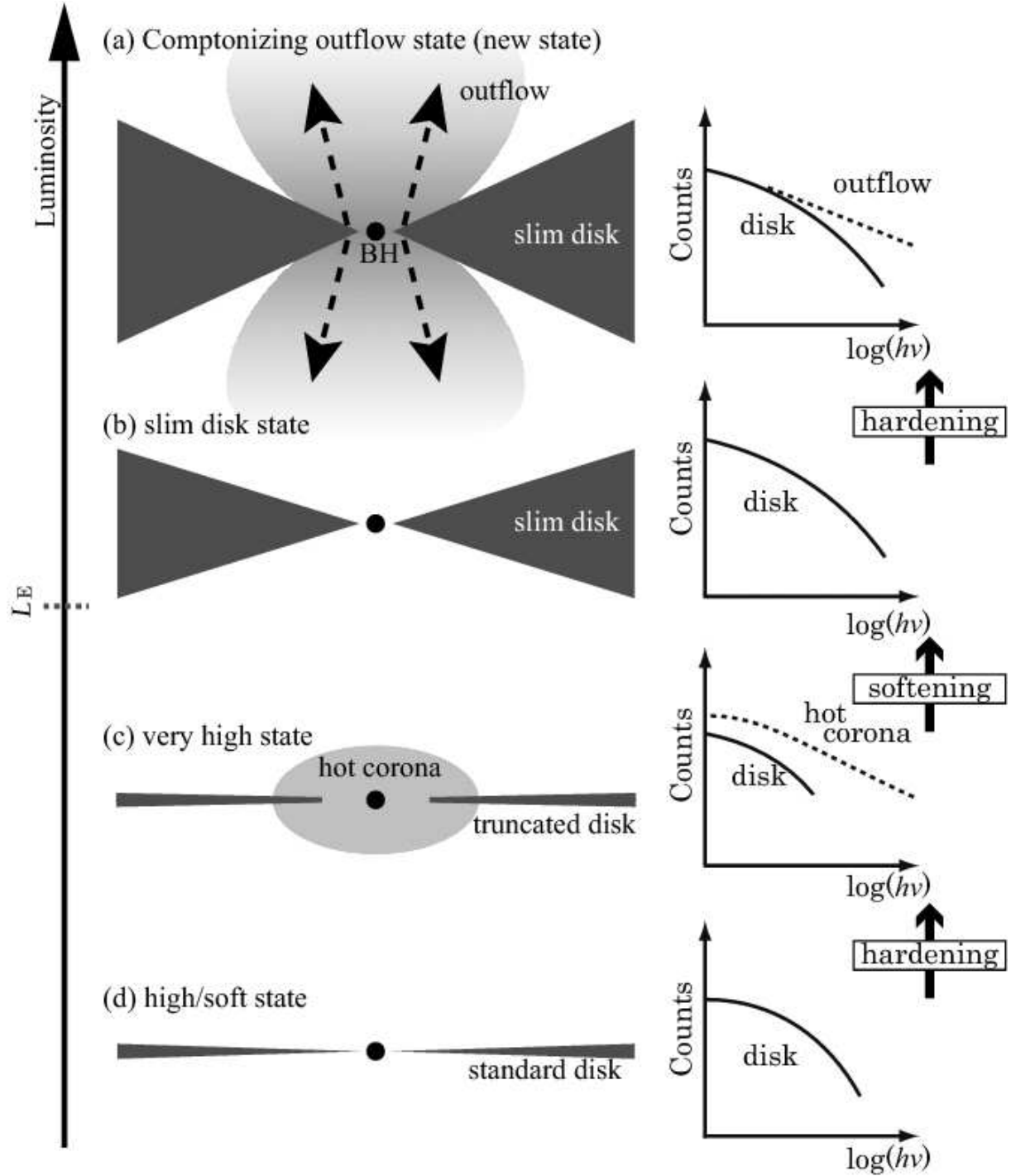


Fig. 4. Schematic pictures of the states of accretion disks. From top to bottom: (a) Comptonizing outflow state, which consists of supercritical accretion flows (i.e., slim disks) and Comptonizing outflows, (b) slim disk state, (c) very high state, and (d) high/soft state. The SED of the new state is harder than that of the slim disk state, because the new state includes a hot outflow which up-scatters seed photons from the underlying disk.